A Novel Fixed Time Supertwisted Integral Synergetic Control for Vehicle-to-Load operation of Electric Vehicles

Hafiz Mian Muhammad Adil, Hassan A. Khan
Dept. of EE, Lahore University of Management Sciences (LUMS)
Lahore, Pakistan
hafiz.adil@lums.edu.pk

Mashood Nasir
Cissoid Semiconductors
1435 Mont-Saint-Guibert, Belgium.
mashood.nasir@cissoid.com

***Abstract*—Vehicle-to-Load (V2L) operation of electric vehicles (EVs) enables their utilization as mobile energy hubs contributing to energy resilience with potential to extending their utility beyond transportation, while complementing grid stability through decentralized load support. However, the efficient utilization of V2L in EVs depends on the robust operation of the power electronic interface between the EV and the load, which necessitates a reliable control design. To enhance the seamless utilization of the V2L operational mode in EVs, this paper proposes a novel fixed-time supertwisted integral synergetic control (FT-STISC), altering the dynamic evolution of synergetic control and hybridizing it with supertwisted action for the boost-based converter interface between the EV and the load. The parameters of the proposed controller are optimally tuned using the whale optimization algorithm (WOA), and an extensive set of simulations is conducted using MATLAB/Simulink to validate the proposed controller under various scenarios, including load power variations and compatibility with different input voltage ranges. The proposed controller, compared to state-of-the-art integral synergetic control (ISC) and sliding mode control (SMC), exhibits enhanced and robust performance, characterized by a faster settling time (2 ms), a lower root mean square error (RMSE) of 0.0007 V, and no chattering. Additionally, the real-time operation of the proposed controller is tested through controller hardware-in-the-loop (C-HIL) validation using the Texas Instruments TMS320F28379D Delfino Launchpad.**

I. Introduction

The growing adoption of electric vehicles (EVs) has diversified their usage into various operational modes, notably vehicle-to-grid (V2G) and vehicle-to-anything (V2X) [1]. Within the V2X framework, the concept of vehicle-to-load (V2L) is gaining prominence due to advancements in transportation electrification, particularly in power electronics. V2L operation extends the role of EVs beyond mobility, enabling them to function as mobile energy sources for diverse electrical loads, ranging form low-power household appliances and communication devices to medium-scale emergency, industrial, and infrastructure systems [2]. These include vehicle-to-home (V2H), vehicle-to-building (V2B), vehicle-to-vehicle (V2V), and vehicle-to-assistance (V2A), all of which fall under the V2L domain. In addition to supporting off-grid and emergency loads, V2L systems can complement grid resilience by providing decentralized energy backup during peak demand or outage scenarios. Fig. 1 illustrates a general representation of V2L operation in an EV.

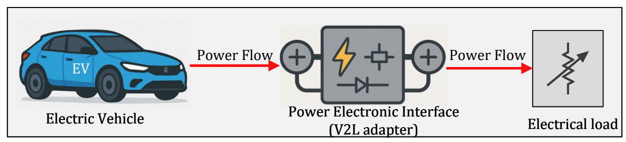

Fig. 1: General representation of V2L operation

An efficient power conditioning unit (electronic interface) is essential for effective V2L operation, to which various control strategies have been explored in literature. In [3], a proportional-integral (PI) control is used for an isolated bidirectional converter serving both DC and AC loads. Similarly, [4] and [5] apply PI control for dual active bridge (DAB) and fault-tolerant boost converters, respectively, in V2X applications. Although widely adopted due to their simplicity, PI controllers suffer from slow dynamic response and limited robustness to load variations. They also struggle to manage the inherent nonlinear behavior of power converter systems, which is crucial under the varying loads typical of V2L operations. A model-free control approach is proposed in [6] for DC-DC LLC converters in V2X settings. It regulates voltage and current using only input-output measurements without requiring a system model. While model-independent, its performance is sensitive to measurement quality and requires frequent parameter tuning, limiting its effectiveness under disturbances. To overcome the limitations of linear and model-free controllers, there has been a recent shift toward nonlinear control methods in V2X applications. Nonlinear controllers offer improved dynamic performance by leveraging the full nonlinear model of the system [7]. However, each method has its own strengths and drawbacks. In [8], a backstepping-based controller enhances performance in a V2H application, but the method is computationally intensive, complex in design, and limited to systems in strict feedback form. Sliding mode control (SMC) is another widely used robust nonlinear method that operates on variable-structure control principles. Various

979-8-3315-8138-1

SMC-based strategies have been proposed [9–11] for V2X (V2H, V2V, V2L) operations. While SMC offers robustness against load variations, its primary drawback is chattering caused by the discontinuous control action, resulting in a variable switching frequency and undesirable heat and power losses in converters [12]. To mitigate this, higher-order SMC variants, such as supertwisting SMC (ST-SMC) and adaptive ST-SMC, have been investigated in [13] and [14], respectively. These controllers reduce chattering by employing continuous control laws while retaining robustness. Another nonlinear technique to eliminate chattering is synergetic control [15]. Similar to SMC in structure, it avoids discontinuous terms and enables control over convergence rate through dynamic evolution. Despite its effectiveness in eliminating chattering, synergetic control exhibits relatively weaker robustness to abrupt load variations, and its convergence is not guaranteed in a fixed time.

To address the above-mentioned challenges, this work has the following contributions:

- A novel fixed-time supertwisted integral synergetic control (FT-STISC) for V2L operation of EVs is proposed, which integrates a hyperbolic tangent-based supertwisting mechanism with fixed-time integral synergetic control. This hybrid approach enhances dynamic response, ensures fixed-time state convergence, and maintains robustness to load changes. The hyperbolic tangent function ensures smooth, continuous control action, eliminating chattering.
- The proposed controller is validated using both simulations and controller hardware-in-the-loop (C-HIL) experiments under varying load conditions and input voltages.
- The superior dynamic response of the proposed controller is benchmarked against conventional SMC and Integral Synergetic Control (ISC).

The remaining paper is structured as follows: Section II presents the mathematical model; Section III describes the control design; Section IV discusses results, comparative response, and C-HIL validation; and Section V concludes the work.

II. V2L SYSTEM MODELLING

The electrical schematic for V2L operation is shown in Fig. 2. A DC-DC boost converter interfaces the EV DC bus with the load, represented by an equivalent resistance R_o. The converter includes an inductance L and output capacitance C, with inductor current i_L and load voltage v_L, respectively. It is pertinent to note that effects like detailed component parasitics, losses, thermal dynamics, and aging effects are not explicitly modelled and will be considered in related future work.

As the converter operates unidirectionally (vehicle to load), switches K and D function complementarily, resulting in the following two operation modes:

$$\underbrace{\begin{matrix} L\dfrac{di_L}{dt} = V_{in} - V_o \\ C\dfrac{dV_o}{dt} = i_L - \dfrac{V_o}{R_o} \end{matrix}}_{(D:On,\ K:Off)} \qquad \underbrace{\begin{matrix} L\dfrac{di_L}{dt} = V_{in} \\ C\dfrac{dV_o}{dt} = -\dfrac{V_o}{R_o} \end{matrix}}_{(D:Off,\ K:On)} \tag{1}$$

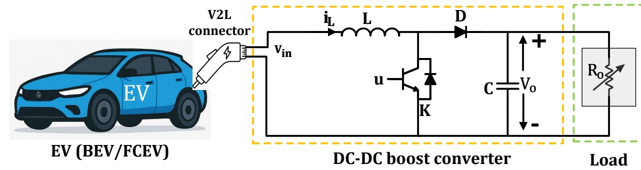

Fig. 2: Electrical schematic of V2L operation via DC-DC boost converter

For control design, the state-space averaged model of the boost converter can be derived using the averaging method as:

$$\begin{cases} \dot{w}_1 = -(1-\mu)\dfrac{w_2}{L} + \dfrac{V_{in}}{L} \\ \dot{w}_2 = (1-\mu)\dfrac{w_1}{C} - \dfrac{w_2}{R_o C} \end{cases} \tag{2}$$

where w_1, w_2, and μ are the averaged inductor current i_L, output voltage v_o, and control input u, respectively.

III. DESIGN AND STABILITY ANALYSIS OF FT-STISC CONTROLLER

The primary goal of the proposed FT-STISC controller is to regulate the load voltage and inductor current to their respective reference values. Its design includes the hybridization of fixed-time integral synergetic control with supertwisting SMC to enhance dynamic response and robustness of the system under varying load and input conditions. The proposed control strategy is inherently scalable and can be employed to multi-converter V2L systems in a decentralized fashion.

A. Design procedure

To achieve the control objectives, define the error functions as:

$$\begin{cases} \kappa_1 = w_1 - w_{1ref} \\ \kappa_2 = w_2 - w_{2ref} \end{cases} \tag{3}$$

where w_{1ref} and w_{2ref} represent the reference values of the inductor current and load voltage, respectively. Using (2), the error derivatives are:

$$\begin{cases} \dot{\kappa}_1 = -(1-\mu)\dfrac{w_2}{L} + \dfrac{V_{in}}{L} - \dot{w}_{1ref} \\ \dot{\kappa}_2 = (1-\mu)\dfrac{w_1}{C} - \dfrac{w_2}{R_o C} - \dot{w}_{2ref} \end{cases} \tag{4}$$

A macro-variable Λ is defined to drive the errors to the invariant manifold $\Lambda = 0$:

$$\Lambda = q_1\kappa_1 + q_2\int_0^t \kappa_1 dt + q_3\kappa_2 + q_4\int_0^t \kappa_2 dt \tag{5}$$

where $q_1, q_2, q_3, q_4 > 0$ are controller parameters. The integral form in (5) enhances steady-state accuracy and reduces overshoot/undershoot, contributing to the fixed-time synergetic control structure.

According to variable control structure theory, the control law is:

$$\mu_{FT-STISC} = \mu_{eq} + \mu_{sw} \tag{6}$$

where μ_{eq} is derived from fixed-time integrative synergetic control, and μ_{sw} is the supertwisting switching part:

$$\mu_{sw} = -\eta_1|\Lambda|^{0.5}tanh(\Lambda) - \int_0^t \eta_2 tanh(\Lambda)dt \tag{7}$$

979-8-3315-8138-1

with $\eta_1, \eta_2 > 0$, and

$$tanh(\Lambda) = \frac{e^{\Lambda} - e^{-\Lambda}}{e^{\Lambda} + e^{-\Lambda}} \tag{8}$$

Unlike the standard supertwisting algorithm, $tanh(\Lambda)$ is used in (7) instead of the signum function to further reduce chattering and ensure the continuous nature of the control law.

To synthesize μ_{eq} in (6), we use the dynamic evolution:

$$T\dot{\Lambda} + \tau(\lambda) = 0 \tag{9}$$

with

$$\tau(\Lambda) = \Lambda^r + \Lambda^{s^{-1}} \tag{10}$$

where $r > 1$, $s > 1$ are odd integers.

Lemma 1 [16]. *The function in (10) satisfies:*
P1: $\tau(\Lambda)$ *is differentiable and invertible*
P2: $\tau(0) = 0$
P3: $\tau(\Lambda)\Lambda > 0 \quad \forall \Lambda \neq 0$

From Lemma 1 and (10), the convergence to $\Lambda = 0$ is guaranteed within fixed time T, with an upper bound:

$$T_{max}(\Lambda) = T\left(\frac{rs - 1}{(r-1)(s-1)}\right) \tag{11}$$

From (5), the derivative $\dot{\Lambda}$ is:

$$\dot{\Lambda} = q_1\dot{\kappa}_1 + q_2\kappa_1 + q_3\dot{\kappa}_2 + q_4\kappa_2 \tag{12}$$

Substituting (12) into (9), we get:

$$T\big(q_1\dot{\kappa}_1 + q_2\kappa_1 + q_3\dot{\kappa}_2 + q_4\kappa_2\big) + \Lambda^r + \Lambda^{s^{-1}} = 0 \tag{13}$$

Using (13) and (4), the equivalent control μ_{eq} becomes:

$$\mu_{eq} = 1 + \frac{N}{D} \tag{14}$$

where

$$N = \left(\frac{-q_1 w_1}{C} + \frac{q_2 w_2}{L}\right) \tag{15}$$

and

$$D = \Bigg(-\frac{\Lambda^r + \Lambda^{s^{-1}}}{T} + \frac{q_1 w_2}{R_o C} + q_1\dot{w}_{2ref} - \frac{q_2 V_{in}}{L} + q_2\dot{w}_{1ref} - q_3\kappa_1 - q_4\kappa_2\Bigg) \tag{16}$$

B. Stability analysis

Theorem: *For the macrovariable* $\Lambda(w)$ *in (5), a Lyapunov function* $L(\Lambda)$ *exists such that the control signal in (14) ensures* $L(\Lambda) < 0$*, establishing asymptotic stability for the system in (2).*

Proof: Define the Lyapunov function:

$$L = 0.5\Lambda^2 \tag{17}$$

Taking its derivative:

$$\dot{L} = \Lambda\dot{\Lambda} \tag{18}$$

Substituting $\dot{\Lambda}$ from (9):

$$\dot{L} = \Lambda\Big(\frac{-\tau(\Lambda)}{T}\Big) \tag{19}$$

Using (10), this becomes:

$$\dot{L} = \frac{-1}{T}\big(\Lambda^{r+1} + \Lambda^{\frac{s+1}{s}}\big) \tag{20}$$

Since $r+1$ and $\frac{s+1}{s}$ are even for odd r, $s > 1$, we have $\dot{L} < 0$, proving asymptotic stability [17].

IV. Results and Discussion

The proposed controller is implemented and validated in the Matlab/Simulink environment. The control implementation layout is shown in Fig. 3, and simulation parameters are listed in Table I. To optimize controller performance, its parameters are tuned using the Whale Optimization Algorithm (WOA) [18], based on the Integral Time Absolute Error (ITAE) criterion, which effectively compensates for both transient and steady-state behavior.WOA offers a balanced exploration-exploitation capability, enabling reliable convergence without extensive parameter tuning. The Fitness function for WOA-based tuning is defined as:

$$F = \int_0^t t(|\kappa_1| + |\kappa_2|)dt \tag{21}$$

TABLE I: Simulation parameters

Parameters	Values
System parameters	
L, C, f_{sw}	$470\mu H$, $1000\mu F$, $100kHz$,
v_{in}, v_{Cref}	$350 - 480V$, $480V$
Controller parameters	
q_1, q_2, q_3, q_4	8, 6, 8, 1
r, s, T	3, 9, 0.00328
η_1, η_2	0.1, 9

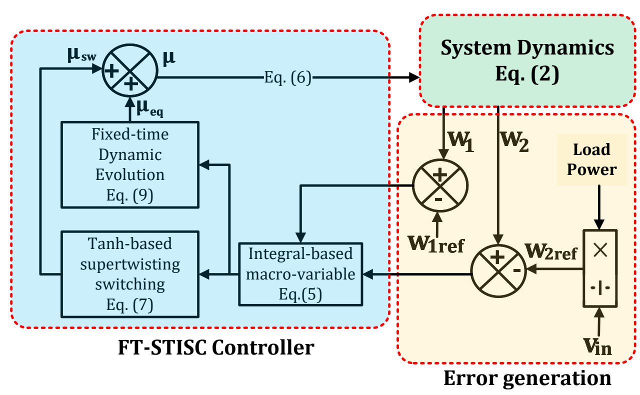

Fig. 3: Control architecture for the system in Fig. 2

The proposed controller is evaluated under four test cases. The system's power capacity is limited to 75 kW, reflecting advancements in EV energy storage, which now reach up to 100 kW. Power levels are varied across the full range to assess V2L performance under low, medium, and high (emergency) scenarios, though actual durations may vary depending on the specific V2L application.

979-8-3315-8138-1

A. Case-1: Increasing Loading Power

In this case, the proposed controller is tested under ascending load power variations as follows:

$$\text{Load Power} = \begin{cases} 15\ kW, & \text{for } 0\ s \leq t \leq 0.4\ s \\ 30\ kW, & \text{for } 0.4\ s \leq t \leq 0.8\ s \\ 45\ kW, & \text{for } 0.8\ s \leq t \leq 1.2\ s \\ 60\ kW, & \text{for } 1.4\ s \leq t \leq 1.6\ s \\ 72\ kW, & \text{for } 1.6\ s \leq t \leq 2\ s \end{cases} \tag{22}$$

The load voltage and inductor current responses are shown in Fig. 4. The load voltage reference is set at 480 V, and perfect voltage regulation is observed. Minor dips occur in response to power demand changes but remain within ± 470 V, staying inside the 2.5% tolerance range. The inductor current also tracks its varying reference accurately, indicating smooth and stable power delivery during V2L operation.

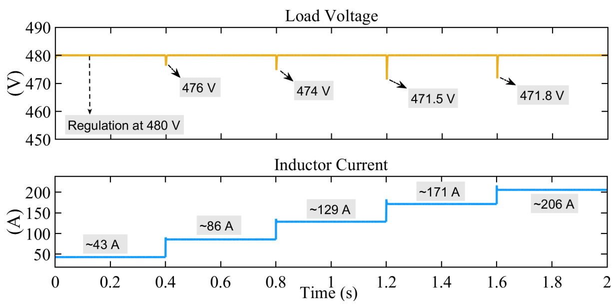

Fig. 4: System response for Case-1.

B. Case-2: Decreasing Loading power

This case validates the proposed controller under a decreasing load power demand, with variations taken as the exact reverse of those in the previous case (Case-1). The tracking responses of the load voltage and inductor current are shown in Fig. 5. The controller maintains accurate voltage regulation and current tracking throughout. Voltage surges remain below 490 V, well within the 2.5% tolerance range.

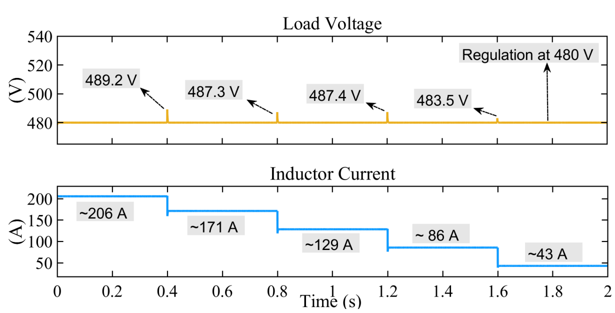

Fig. 5: System response for Case-2.

C. Case-3: Mixed Input Voltage

In this case, the proposed controller is tested under varying input voltage levels. The voltage regulation response is shown in Fig. 6. The controller maintains a load voltage of 480 V across all cases. Surges during input voltage changes remain within 2 V, i.e., within 0.5% of the regulated level.

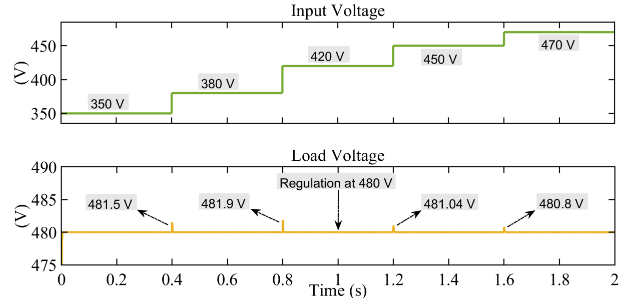

Fig. 6: System response for Case-3.

D. Case-4: Comparative response with mixed load power

A comparative analysis of load-voltage regulation is carried out between the proposed controller and the established SMC and ISC methods to highlight the performance improvements achieved. Fig. 7 shows the load power profile, deliberately designed to include both increasing and decreasing levels at 0.4 s intervals, and the voltage regulation responses of the three controllers.

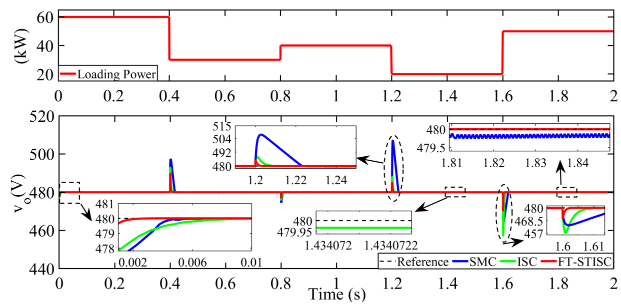

Fig. 7: Comparative response with mixed loading power.

The proposed FT-STISC controller achieves the fastest convergence (0.002 s), while ISC is the slowest (0.009 s). SMC settles at 0.006 s but suffers from chattering, visible in the zoomed-in view of Fig. 7. In contrast, both ISC and FT-STISC are free from chattering. ISC has no discontinuous term involved in its design, while FT-STISC has a continuous nature of the switching term, aided by the use of *tanh* function. The proposed controller also ensures tighter voltage regulation with zero steady-state error (up to three decimal places), compared to ISC (0.02 V) and SMC (0.2 V). Moreover, SMC shows larger surges and slower recovery than ISC and FT-STISC. The proposed controller exhibits an over/under-shoot of ± 10 V, within the $\pm 2.5\%$ tolerance. In contrast, SMC and ISC show larger transients and slower retracing. A quantitative comparison is presented in Table II.

TABLE II: Quantitative comparison

	Settling time (s)	RMSE (V)	Chattering
SMC	0.006	0.9443	Yes
ISC	0.009	0.7960	No
FT-STISC	0.002	0.0007	No

Fig. 8 illustrates the Controller Hardware-in-the-Loop (C-HIL) configuration used to validate the proposed controller in

979-8-3315-8138-1

real time. The implementation employs the Texas Instruments C2000 Delfino TMS320F28379D LaunchPad as the control platform. The controller algorithm is deployed on the microcontroller, while the corresponding system model is executed within MATLAB/Simulink. Communication between the host computer and the controller is established through the serial communication interface (SCI) for transmitting feedback and control signals. The dynamic load-response results, presented in Fig. 9, confirm the controller's capability to regulate output voltage effectively under varying load conditions, demonstrating its practical real-time applicability.

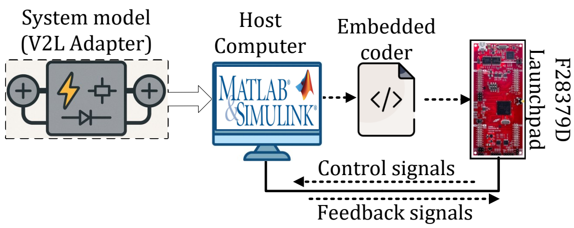

Fig. 8: C-HIL validation setup.

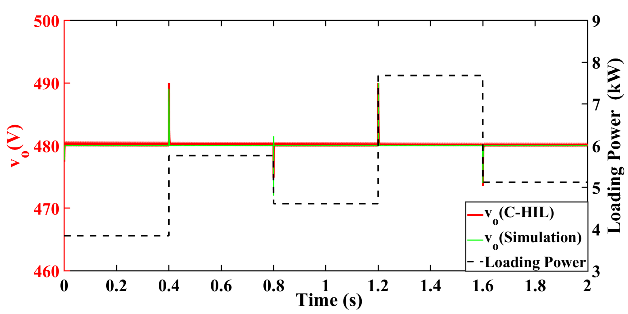

Fig. 9: Voltage tracking response under C-HIL validation.

V. Conclusion

By incorporating the supertwisted action into the altered fixed-time-based dynamic evolution of synergetic control, a novel robust nonlinear control strategy is proposed in this work, ensuring seamless V2L operation for electric vehicles and enhancing their potential role in decentralized energy support and grid resilience. The proposed control approach is Lyapunov stable and exhibits enhanced system dynamic response in terms of output voltage regulation and inductor current reference tracking, thereby facilitating efficient power transfer from an electric vehicle to a load during V2L operations. Both simulations and CHIL validations are performed, and the results demonstrate the superior performance of the proposed controller compared to sliding mode and integral synergetic controllers. The key performance indicators (zero steady-state error, nil chattering, and faster convergence: 2 ms) confirm the viability of the proposed controller as an effective driver for the vehicle-load power converter interface. Future work will include barrier-based adaptation of the controller parameters and the implementation of anti-windup techniques to further enhance performance.

References

[1] M. A. Rehman, M. Numan, H. Tahir, U. Rahman, M. W. Khan, and M. Z. Iftikhar, "A comprehensive overview of vehicle to everything (V2X) technology for sustainable EV adoption," *Journal of Energy Storage*, vol. 74, p. 109304, 2023.

[2] R. Khezri, D. Steen, *et al.*, "A review on implementation of vehicle to everything (V2X): Benefits, barriers and measures," in *2022 IEEE PES Innovative Smart Grid Technologies Conference Europe (ISGT-Europe)*, pp. 1–6, IEEE, 2022.

[3] X. Wang, Y. Liu, W. Qian, A. Janabi, B. Wang, X. Lu, K. Zou, C. Chen, and F. Z. Peng, "Design, and control of a SiC isolated bidirectional power converter for V2L applications to both DC and AC load," in *2019 IEEE 7th workshop on wide bandgap power devices and applications (WiPDA)*, pp. 143–150, IEEE, 2019.

[4] Y. Liu, X. Wang, W. Qian, A. Janabi, B. Wang, X. Lu, K. Zou, C. Chen, and F. Z. Peng, "DC voltage control of inverter interfaced dual active bridge converter for V2L applications," in *2019 IEEE 7th workshop on wide bandgap power devices and applications (WiPDA)*, pp. 319–324, IEEE, 2019.

[5] M. A. Rodriguez Licea, "Fault tolerant boost converter with multiple serial inputs and output voltage regulation for vehicle-to-aid services," *Energies*, vol. 13, no. 7, p. 1694, 2020.

[6] H. Al Attar, M. Hamida, M. Ghanes, and M. Taleb, "Model free control design of DC-DC LLC converter with phase shift modulation in V2X mode for EV charger application," in *2022 IEEE Conference on Control Technology and Applications (CCTA)*, pp. 734–739, IEEE, 2022.

[7] M. Batool, W. Hassan, and D. D.-C. Lu, "Review of advanced control strategies for isolated DC-DC converters in DC microgrids," *IEEE Access*, 2025.

[8] E. Saidi, A. Rachid, H. Bella, N. Errifai, and S. Khamlichi, "Nonlinear control of a bidirectional DC-DC power converter in V2H applications," in *International Conference on Digital Technologies and Applications*, pp. 527–535, Springer, 2024.

[9] R. Wang, Q. Sun, C. Sun, H. Zhang, Y. Gui, and P. Wang, "Vehicle-vehicle energy interaction converter of electric vehicles: A disturbance observer based sliding mode control algorithm," *IEEE Transactions on Vehicular Technology*, vol. 70, no. 10, pp. 9910–9921, 2021.

[10] M. İnci, M. Büyük, and N. S. Özbek, "Sliding mode control for fuel cell supported battery charger in vehicle-to-vehicle interaction," *Fuel Cells*, vol. 22, no. 5, pp. 212–226, 2022.

[11] M. İnci and N. S. Özbek, "A novel predictive current sliding mode control for improving the performance efficiency of fuel cell vehicle-to-load (V2L) system with boost converter," *International Journal of Hydrogen Energy*, vol. 138, pp. 973–984, 2025.

[12] L. Wu, J. Liu, S. Vazquez, and S. K. Mazumder, "Sliding mode control in power converters and drives: A review," *IEEE/CAA Journal of Automatica Sinica*, vol. 9, no. 3, pp. 392–406, 2021.

[13] I. Ahmed, H. M. M. Adil, S. Ahmed, I. Ahmad, and Z. Rehman, "Robust nonlinear control of battery electric vehicle charger in grid to vehicle and vehicle to grid applications," *Journal of Energy Storage*, vol. 52, p. 104813, 2022.

[14] H. Al Attar, M. Hamida, M. Ghanes, and M. Taleb, "Electric vehicle charger control design combining phase shift modulation with an adaptive super twisting algorithm," in *2022 16th International Workshop on Variable Structure Systems (VSS)*, pp. 135–140, IEEE, 2022.

[15] A. Z. M. Gaid, A.-K. Hamid, and M. M. Farag, "High gain multilevel boost converter-based synergetic MPPT controller for standalone photovoltaic array," in *2025 7th International Youth Conference on Radio Electronics, Electrical and Power Engineering (REEPE)*, pp. 1–7, IEEE, 2025.

[16] S. Achour, K. Mokhtari, and A. Rahmoune, "Quadrotor attitude control with a modified fixed-time synergetic controller: A geometric analysis and experimental validation," *Asian Journal of Control*, vol. 27, no. 2, pp. 1051–1067, 2025.

[17] H. M. M. Adil and H. A. Khan, "A novel hybrid nonlinear control of four switch buck-boost converter feeding constant power load in fuel cell-based DC microgrid," *Results in Engineering*, p. 105490, 2025.

[18] H. M. M. Adil and H. A. Khan, "WOA-tuned supertwisted synergetic control of multipurpose on-board charger for G2V/V2G/V2V operational modes of electric vehicles," *Control Engineering Practice*, vol. 154, p. 106136, 2025.

979-8-3315-8138-1